Seebeck nanoantennas for the detection and characterization of infrared radiation

Edgar Briones,[1] Alexander Cuadrado,[2] Joel Briones,[3] Ramón Díaz de León,[4] Juan Carlos Martínez-Antón,[2] Stefan McMurtry,[5] Michel Hehn,[5] François Montaigne,[5] Javier Alda,[2] and Francisco Javier González[1,*]

[1]*Coordinación para la Innovación y la Aplicación de la Ciencia y la Tecnología, Universidad Autónoma de San Luís Potosí, Sierra Leona 550, Lomas 2a Sección, SLP, México*
[2]*Applied Optics Complutense Group, University Complutense of Madrid, Faculty of Optics and Optometry, C/ Arcos de Jalón, 118. 28037, Madrid, Spain*
[3]*Departamento de Física, Universidad de Santiago de Chile (USACH), 9170124 Santiago, Chile*
[4]*Instituto Tecnológico de San Luis Potosí, Av. Tecnológico, S/N Col UPA, Soledad de Graciano Sánchez, México*
[5]*Institut Jean Lamour, CNRS, Université de Lorraine, Bd des Aiguillettes, BP70239, F-54506 Vandoeuvre Les Nancy, France*
[*]*javier.gonzalez@uaslp.mx*

Abstract: Arrays of metallic thermocouples in the shape of spiral nanoantennas are proposed as infrared detectors, which use the thermoelectric properties of the metallic interfaces to generate electrical DC signals. The responsivity of these types of antennas is evaluated from both theoretical and numerical perspectives pointing out its potential as infrared sensors. Moreover, the same structures can be used to characterize the state of polarization of the optical near fields with a spatial resolution comparable to the wavelength.

OCIS codes: (040.3060) Infrared; (040.5570) Quantum detector.

References and links

1. P. Mühlschlegel, H. J. Eisler, O. J. F. Martin, B. Hecht, and D. W. Pohl, "Resonant Optical Antennas," Science **308**(5728), 1607–1609 (2005).
2. L. Novotny and N. van Hulst, "Antennas for light," Nat. Photonics **5**(2), 83–90 (2011).
3. W. L. Barnes, A. Dereux, and T. W. Ebbesen, "Surface plasmon subwavelength optics," Nature **424**(6950), 824–830 (2003).
4. F. Neubrech, T. Kolb, R. Lovrincic, G. Fahsold, A. Pucci, J. Aizpurua, T. W. Cornelius, M. E. Toimil-Molares, R. Neumann, and S. Karim, "Resonances of individual metal nanowires in the infrared," Appl. Phys. Lett. **89**(25), 253104 (2006).
5. R. L. Olmon, P. M. Krenz, A. C. Jones, G. D. Boreman, and M. B. Raschke, "Near-field imaging of optical antenna modes in the mid-infrared," Opt. Express **16**(25), 20295–20305 (2008).
6. S. Vedantam, H. Lee, J. Tang, J. Conway, M. Staffaroni, and E. Yablonovitch, "A plasmonic dimple lens for nanoscale focusing of light," Nano Lett. **9**(10), 3447–3452 (2009).
7. P. Biagioni, J. S. Huang, and B. Hecht, "Nanoantennas for visible and infrared radiation," Rep. Prog. Phys. **75**(2), 024402 (2012).
8. G. A. E. Vandenbosch and Z. Ma, "Upper bounds for the solar energy harvesting efficiency of nano-antennas," Nano Energy **1**(3), 494–502 (2012).
9. Z. Ma and G. A. E. Vandenbosch, "Optimal solar energy harvesting efficiency of nano-rectenna systems," Sol. Energy **88**, 163–174 (2013).
10. D. Dregely, R. Taubert, J. Dorfmüller, R. Vogelgesang, K. Kern, and H. Giessen, "3D optical Yagi-Uda nanoantenna array," Nat Commun **2**, 267 (2011).
11. F. J. González, B. Ilic, J. Alda, and G. D. Boreman, "Antenna-Coupled Infrared Detectors for Imaging Applications," IEEE J. Sel. Top. Quantum Electron. **11**(1), 117–120 (2005).
12. C. Fumeaux, M. A. Gritz, I. Codreanu, W. L. Schaich, F. González, and G. D. Boreman, "Measurement of the resonant lengths of infrared dipole antennas," Infrared Phys. Technol. **41**(5), 271–281 (2000).
13. F. González and G. Boreman, "Comparison of dipole, bowtie, spiral and log-periodic IR antennas," Infrared Phys. Technol. **46**(5), 418–428 (2005).
14. P. Krenz, J. Alda, and G. Boreman, "Orthogonal infrared dipole antenna," Infrared Phys. Technol. **51**(4), 340–343 (2008).
15. C. Fumeaux, W. Herrmann, F. Kneubühl, and H. Rothuizen, "Nanometer thin-film Ni-NiO-Ni diodes for detection and mixing of 30 THz radiation," Infrared Phys. Technol. **39**(3), 123–183 (1998).

#212448 - $15.00 USD Received 20 May 2014; revised 11 Jul 2014; accepted 14 Aug 2014; published 17 Sep 2014

16. S. Rockwell, D. Lim, B. A. Bosco, J. H. Baker, B. Eliasson, K. Forsyth, and M. Cromar, "Characterization and modeling of metal/double-insulator/metal diodes for millimeter wave wireless receiver applications", in *Proceeding of IEEE Radio Frequency Integrated Circuits Symposium*, (Honolulu, HI, 2007), pp. 171–174.
17. S. Grover and G. Moddel, "Engineering the current–voltage characteristics of metal–insulator–metal diodes using double-insulator tunnel barriers," Solid-State Electron. **76**(1), 94–99 (2012).
18. N. Alimardani and J. F. Conley, Jr., "Step tunneling enhanced asymmetry in asymmetric electrode metal-insulator-insulator-metal tunnel diodes," Appl. Phys. Lett. **102**(14), 143501 (2013).
19. J. A. Bean, B. Tiwari, G. H. Bernstein, P. Fay, and W. Porod, "Thermal infrared detection using dipole antennacoupled metal-oxide-metal diodes," J. Vac. Sci. Technol. B **27**(1), 11–14 (2009).
20. E. Briones, J. Alda, and F. J. González, "Conversion efficiency of broad-band rectennas for solar energy harvesting applications," Opt. Express **21**(3), A412–A418 (2013).
21. Z. Zhu, S. Joshi, S. Grover, and G. Moddel, "Graphene geometric diodes for terahertz rectennas," J. Phys. D Appl. Phys. **46**(18), 185101 (2013).
22. U. Dillner, E. Kessler, and H.-G. Meyer, "Responsivity and detectivity modeling of thermal radiation sensors based on a biased thermocouple," J. Phys. D Appl. Phys. **44**(30), 305102 (2011).
23. G. P. Szakmany, P. M. Krenz, A. O. Orlov, G. H. Bernstein, and W. Porod, "Antenna-Coupled Nanowire Thermocouples for Infrared Detection," IEEE Trans. NanoTechnol. **12**(2), 163–167 (2013).
24. G. P. Szakmany, P. M. Krenz, L. C. Schneider, A. O. Orlov, G. H. Bernstein, and W. Porod, "Nanowire Thermocouple Characterization Platform," IEEE Trans. NanoTechnol. **12**(3), 309–313 (2013).
25. M. Bareis, P. M. Krenz, G. P. Szakmany, B. N. Tiwari, D. Kalblein, A. O. Orlov, G. H. Bernstein, G. Scarpa, B. Fabel, U. Zschieschang, H. Klauk, W. Porod, and P. Lugli, "Rectennas Revisited," IEEE Trans. NanoTechnol. **12**(6), 1144–1150 (2013).
26. D. M. Rowe, *Thermoelectrics Handbook: Macro to Nano* (Taylor and Francis, 2006).
27. A. Graf, M. Arndt, M. Sauer, and G. Gerlach, "Review of micromachined thermopiles for infrared detection," Meas. Sci. Technol. **18**(7), R59–R75 (2007).
28. C. Fumeaux, G. D. Boreman, W. Herrmann, H. Rothuizen, and F. K. Kneubühl, "Polarization response of asymmetric-spiral infrared antennas," Appl. Opt. **36**(25), 6485–6490 (1997).
29. L. J. A. Kaiser, "The Archimedean two-wire spiral antenna," IRE Trans. Antennas Propag. **8**(3), 312–323 (1960).
30. C. A. Balanis, *Antenna Theory* (John Willey and Sons, 1997).
31. E. D. Palik, *Handbook of Optical Constants of Solids 3* (New York, USA, 1997).
32. G. Baffou, C. Girard, and R. Quidant, "Mapping Heat Origin in Plasmonic Structures," Phys. Rev. Lett. **104**(13), 136805 (2010).
33. J. Alda, C. Fumeaux, I. Codreanu, J. A. Schaefer, and G. D. Boreman, "Deconvolution method for two-dimensional spatial-response mapping of lithographic infrared antennas," Appl. Opt. **38**(19), 3993–4000 (1999).
34. F. J. González, "Thermal-impedance simulations of antenna-coupled microbolometers," Infrared Phys. Technol. **48**(3), 223–226 (2006).
35. W. Ma and X. Zhang, "Study of the thermal, electrical and thermoelectric properties of metallic nanofilms," Int. J. Heat Mass Transfer **58**(1-2), 639–651 (2013).
36. K. Ono and R. O. Suzuki, "Thermoelectric power generation: Converting low-grade heat into electricity," JOM **50**(12), 49–51 (1998).
37. J. P. Carmo, L. M. Gonçalves, and J. H. Correia, *Micro and Nanodevices for Thermoelectric Converters*, in *Scanning Probe Microscopy in Nanoscience and Nanotechnology 2* (Springer, Berlin, 2012).

1. Introduction

Nanoantennas are resonant metallic structures that provide a way to confine the optical energy into sub-wavelength volumes with a high level of control [1,2]. These nanostructures take advantage of the wave nature of the radiation in order to induce a resonant current along its structure that confines the optical energy [3–5], opening this manner a new route to sense, manipulate and harvest the infrared and visible wavelengths [6–9].

In the far-infrared regime, the introduction of antennas to sense the thermal wavelengths has led to the development of infrared (IR) image acquisition systems and harvesting devices of novel functionalities [10,11]. First antenna thermal detectors have used coupled niobium micro-bolometers in order to introduce substantially faster detectors than the bulk-bolometers at the time (μs), showing efficiencies around 0.01% [12–14]. Meanwhile, the substitution of micro-bolometers by THz nano-rectifiers (based on metal-insulator-metal or metal-insulator-insulator-metal tunnel barriers [15–19]) had added to the antennas the capability to harvest the optical energy. These so-called rectifying antennas were experimentally realized and employed to detect the infrared and visible wavelengths with success, albeit for harvesting applications was not the case. In spite of its attractive recovering efficiency that is claimed to be 100% [8,9], rectifying antennas present major inconvenient due to its low-performance, which to our acknowledge reach efficiencies values of 10^{-9} and 10^{-12} percent for the most

#212448 - $15.00 USD Received 20 May 2014; revised 11 Jul 2014; accepted 14 Aug 2014; published 17 Sep 2014

explored barrier [20]. The match between diodes and the antennas, and the diode-like behavior of the tunnel barriers are self-dependent key parameters that should be improved to increase the performance of devices [8,9]. By the other hand, the incorporation of nano-rectifiers to the antennas (whose dimensions are demanded to be around 60 nm x 80 nm for THz rectification [19]) requires the use of multi-level e-beam lithography processes what can conduce to not-reproducible results. In order to incorporate antennas for harvesting applications, different mechanism other than direct rectification should be explored. Geometric rectification has been proposed as an alternative way to overcome these difficulties using graphene-based devices [21].

In this contribution, we propose a different infrared sensor based on the thermoelectric effect using optical nanoantennas. It permits to overcome, or forget the transfer energy constraint (or mismatch impedance) between the antennas and coupled fast rectifiers, increase the efficiency of devices and reduce the technological problems arising from fabrication. The proposed IR nanoantennas combine the optical properties of antennas to capture radiation with the use of the Seebeck effect as the transduction mechanism. Especially for null or very low bias, the response of thermoelectric IR detectors is potentially very advantageous. The work of Dillner et al [22] shows that sensor detectivity (D*) can be several orders of magnitude higher in IR detectors based on the Seebeck effect. On the other hand, recent contributions has shown the capabilities of this transduction mechanism [23,24] and even state that Seebeck effect is responsible for the signal in Metal-Oxide-Metal devices failing to tunnel the generated currents [25].

The proposed IR sensors consist of series arrangements of nano-thermocouples in the shape of antennas sized to absorb the thermal wavelengths around 10.6 μm. When the structures are illuminated, the resonant current causes a thermal gradient inside the structures (by Joule heating) that leads the thermocouples to generate a Seebeck voltage at the open ends [26, 27]. This signal is given by [27]:

$$V_{OC} = \sum_{n} (S_A - S_B) \cdot \Delta T_n, \tag{1}$$

where n is the number of thermocouples in the stack, $\Delta T_n = T_{Hn}$-T_{Cn} the temperature difference between the hot and cold points of the n-th thermocouple and S_A and S_B the Seebeck coefficients of the materials used in the thermocouple arms [26].

In this work, we determine the Seebeck voltage and responsivity of a series of infrared devices from both numerical and theoretical perspectives showing its potential for infrared sensing. We choose as proof of concept three types of spiral nanoantennas, currently used to sense and retrieve optical energy at a wavelength of 10.6 μm [13, 28].

2. Numerical simulations

2.1 Devices

A sketch of the infrared detectors is shown in Fig. 1 (a)-(c). The detector integrates a square spiral (Fig. 1(a)) and a single loop nanoantenna (Fig. 1(c)) that are sensitive to linear polarized radiation, and an array of Archimedean spiral antennas (Fig. 1(b)) that detect right and left-handed circularly polarized radiation.

#212448 - $15.00 USD Received 20 May 2014; revised 11 Jul 2014; accepted 14 Aug 2014; published 17 Sep 2014

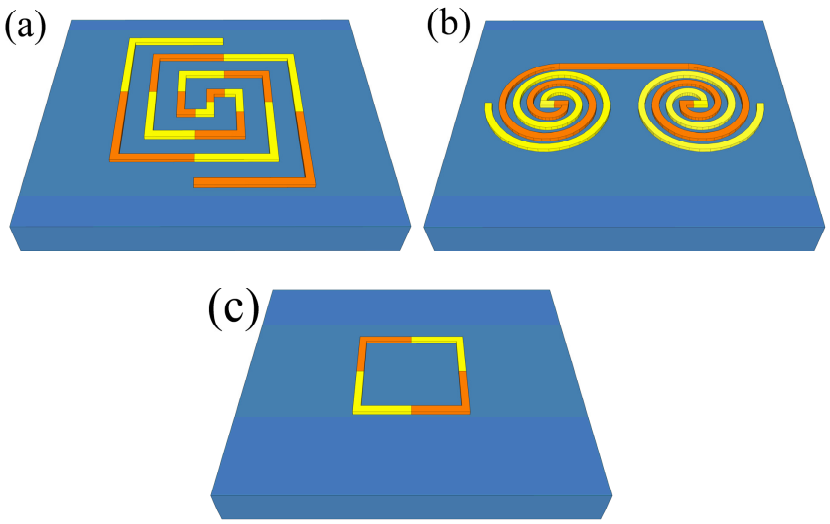

Fig. 1. Schematic diagram of the proposed Seebeck spiral nanoantennas, (a) Square spiral configuration, (b) Archimedean spiral array and (c) Single closed-loop nanoantenna.

The square spiral (Fig. 1(a)) is composed by two symmetrical arms 2.4 μm long (200 nm x 100 nm cross section), which are made out of seven linear elements L_n, whose length is given by:

$$L_n = \begin{cases} a, \text{ for } n = 1, \\ 2a(n-1), \text{ for } n = 2,3,... \end{cases} \quad (2)$$

and an 8th element of 2.8 μm long (where a = 400nm). All the linear elements were split in two parts (except the first and last one) in order to form thermocouples with *L*-shape arms, whose interfaces are parallel to the axes.

The Archimedean array (Fig. 1(b)) is composed of a left-handed and a right-handed spiral connected by the extremes and separated from centers by a distance of 4 μm. The arms of the spirals are described by the following linearly proportional relationships:

$$r = r_0\varphi + r_1 \text{ and } r = r_0(\varphi - \pi) + r_1, \quad (3)$$

where the proportionality constant r_0 is determined by the width w of each arm by $w/2\pi$ (here, w is set at 200 nm) and r_1 denotes the inner radius of the spirals (set at 200 nm) [29]. The arms of both spirals are fabricated with two types of metals in order to form the arrangement shown in Fig. 1(b). Finally, Fig. 1(c) shows a single square closed-loop composed by four linear elements of 2.8 μm long [30] and a cross section of 200 nm x 100 nm.

The considered materials are titanium and nickel (colors yellow and orange, respectively) metals that show an appropriate difference in the values of their Seebeck coefficient, property that determines the performance of materials to generate voltage from heat. By the other hand, metals show a low thermal conductivity [26], allowing the thermocouples to reach a substantial temperature increase and so, to enhance the response of thermocouple given by the relationship (1). The structures were placed on a semi-infinite SiO_2 substrate and a 10.6 μm wavelength plane-wave was used for far-field illumination (with an irradiance of 117 W/cm^2).

The modeling of the structures was performed by using the software package COMSOL Multi-physics (ver3.5a) which provides a good multi-physics platform where both electromagnetic and thermal domains are fully integrated. The numerical model was built using all the optical, thermal and thermo-electrical properties of materials reported at a 10.6 μm wavelength [31].

#212448 - $15.00 USD Received 20 May 2014; revised 11 Jul 2014; accepted 14 Aug 2014; published 17 Sep 2014

2.2 Model

As a first step we evaluated the thermal behavior of the devices by considering the antennas as heat sources when illuminated. For this purpose we determined the increase in temperature by Joule heating due to the optically induced currents. The heat-power density ($q(\boldsymbol{r})$ [W/m^3]) was evaluated inside the volume of the nanoantennas by using [32]:

$$q(r) = 1/2 \cdot \sigma(\omega) \cdot |\vec{E}(r)|^2 \tag{4}$$

where $\sigma(\omega)$ is the conductivity of the material at the frequency of the incident wave ω and is $E(\mathrm{r})$ the distribution of the electric field inside the nanoantennas.

The power density was then used as a source of heat into the solver in order to determine the steady-state temperature distribution, $T(\mathrm{r})$, inside and outside the resonant metallic structures. The temperature changes were calculated by solving the heat transfer equation:

$$\begin{aligned} \nabla \cdot (\kappa \nabla T(r)) &= -q(r), \text{ inside the antennas} \\ \nabla \cdot (\kappa \nabla T(r)) &= 0, \text{ outside the antennas.} \end{aligned} \tag{5}$$

The temperature increase of the junction ΔT is found from the thermal simulations and used to evaluate the voltage response of the antenna by using Eq. (1), as well as the Seebeck coefficient values of 7.2 μV/K and −19.5 μV/K, for nickel and titanium, respectively. Finally, the responsivity exhibited by the thermo-electric nano-antennas was evaluated by:

$$\Re_V = \frac{V_{OC}}{P_{inc}}, \tag{6}$$

where P_{inc} is the power that antennas receive, determined with the effective collection area of the antennas and the irradiance of the incidence beam. Scanning a known irradiance profile over the antenna and registering the signal obtained from it can properly determine this effective area. After deconvolving the signal map, the effective collection area is obtained [33]. A conservative value of this parameter is around λ^2, although smaller values ($\approx 0.1 \times \lambda^2$) have been reported [13].

Even though the thermal-optical analysis is performed by a classical treatment (neither the thermal nor the electric contribution arising from the interfaces are taken into account), this method has shown to give accurate results for thermal-optical analysis of nanoantenna-coupled-bolometers [34, 35].

3. Results

The three arrangements of Seebeck nanoantennas presented in this paper (see Fig. 1) are illuminated for several polarization states, as it was mentioned in section II.

The first element to consider is the square spiral antenna shown in Fig. 1.(a). It has been tested for three different polarizations: circular polarization (right-handed, RCP), and linear polarization along the X (horizontal, LP 0°) and Y (vertical, LP 90°) axis of the square. This square contains 13 Ni-Ti junctions. In order to have it operational and provide an open circuit voltage we have to choose pairs of these junctions. As expected, the hot and cold character of the junctions changes with polarization. Figure 2 shows the temperature map for three polarization states. We have also represented the profile of temperature along the structure. The locations of the junctions are marked with vertical lines. The locations #1 and #15 are the terminal points and are not considered. There are two possible choices, A and B, for the pairs of junctions used to deliver a given voltage from the spiral. Choice A begins with pair 2-3 and choice B begins with pair 3-4. The difference in temperature for these two possible choices is plotted in the bottom of Fig. 2 for the three states of polarization simulated here. This difference in temperature is the responsible for the Seebeck voltage obtained from the successive contribution of thermopairs connected in series.

#212448 - $15.00 USD Received 20 May 2014; revised 11 Jul 2014; accepted 14 Aug 2014; published 17 Sep 2014

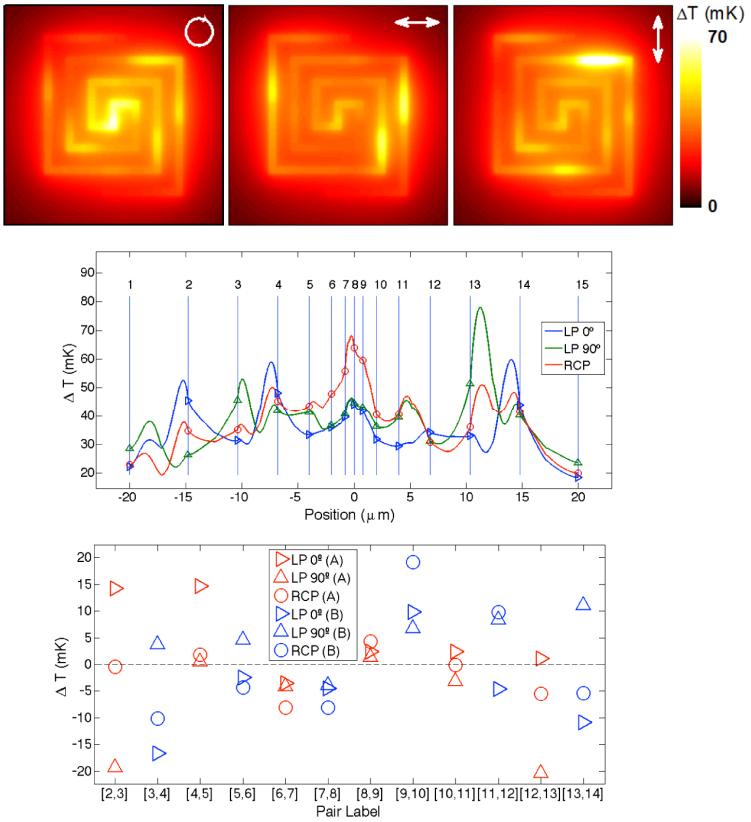

Fig. 2. Top: Temperature map of three different spiral nanoantennas due to Joule heating when illuminated under different polarizations (taken in a plane at the mid-height of structures, z = 50nm). Middle: Temperature profile along the arms of the square spiral nanoantenna. Junctions are represented as vertical lines and numbered being junction #8 the one located at the center of the structure. Bottom: Differences in temperature for the three states of polarization considered and for the two possible choices to produce a Seebeck voltage.

From the previous figure we can see that the system can be tailored to have all the temperature differences having the same sign for the same polarization, for example by eliminating some of the junctions at the center of the structure. Both choices of the junctions contain temperature differences, located at the central region of the antenna which diminishes the magnitude of the Seebeck voltages. If this system is used to provide a signal sensitive to the linear polarization we have to calculate the voltages provided by this arrangement. The results are summarized in Table 1.

Table 1. Voltage Response of the Square Spirals Thermocouples

Voltage (μV)	RHCP	LP 0°	LP 90°
Choice A	–0.1768	0.6877	–0.9952
Choice B	0.0247	–0.6526	0.6841

Figure 3 shows the temperature profile for both elements of the Archimedean spiral nano antenna array which is sensitive to circular polarization. The thermoelectric junctions are localized at the center of the spirals. The hot junction corresponds to the spiral having the helix orientation in the same direction as the incoming polarization. The difference in temperature is 172.3 mK which provides a Seebeck voltage of 3.82 μV. Assuming an irradiance of 117 W/cm^2 and an effective area of approximately 25 μm^2 calculated as twice

#212448 - $15.00 USD Received 20 May 2014; revised 11 Jul 2014; accepted 14 Aug 2014; published 17 Sep 2014

the effective area of a single nanoantenna [13], the responsivity of a single element would be 112 mV/W.

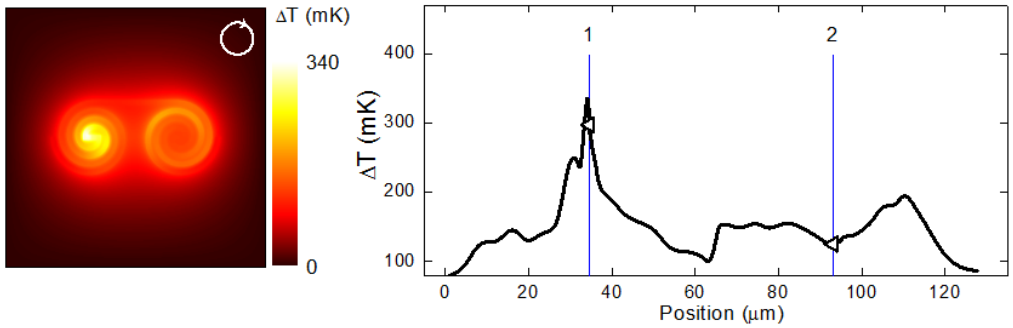

Fig. 3. Temperatures map (right) and profile (left) for the Archimedean spiral for right-handed circular polarization.

The square closed-loop geometry (Fig. 1(c)) shows a distinctive behavior when impinged with different linear polarization orientations. Figure 4 shows the temperature map (right) and profile along the loop (left). Temperature profile generates a voltage difference between the metal junctions that is polarization dependent. From the results, we can see that horizontal and vertical polarizations produce positive and negative alternating voltages respectively. This is caused by the interchanged role of the hot and cold junctions when changing the orientation of the incoming electric field. The case of horizontal (0°) and vertical polarization (90°) provides a voltage almost three orders of magnitude larger than for the 45° and 135° degree orientations. This is due to the symmetry of the arrangement and the location of the junctions. The Seebeck voltage should be extracted by opening the loop at some given location.

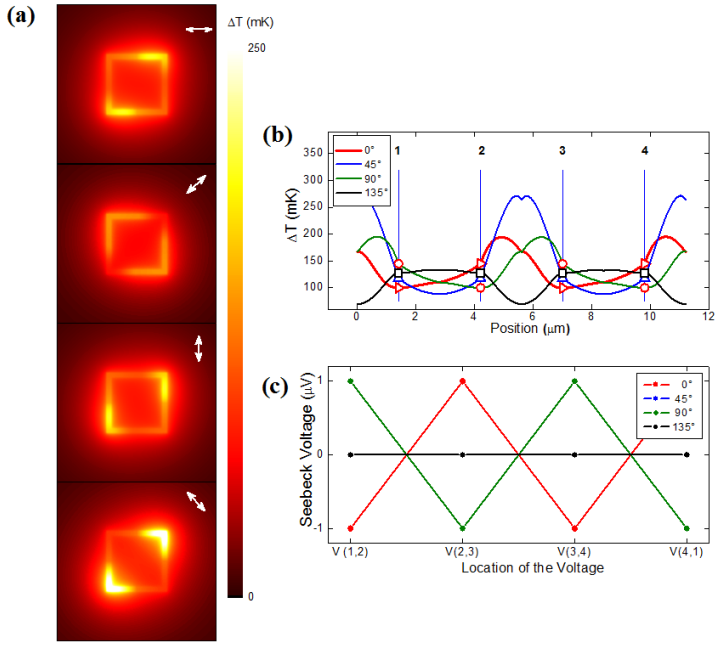

Fig. 4. (a) temperature maps of the square closed-loop single antenna for four different polarization states; (b) temperature profile of the square closed-loop single antenna and (c) Voltage values for several choices of consecutive junctions; the dots represent the voltage

#212448 - $15.00 USD Received 20 May 2014; revised 11 Jul 2014; accepted 14 Aug 2014; published 17 Sep 2014

values for several choices of consecutive junctions. The connecting lines are only presented to group the values for the four different polarizations states.

The responsivity of nanoantennas at 10.6 μm thermal wavelengths was evaluated by considering them as isolated systems. Albeit, in order to integrate them into signal acquisition systems, as the IR imagining device presented in ref. 11, some considerations must be taken into account. First, the thermal impedance of the electric contacts must be higher than that of the antennas in order to prevent the heat exchange between both elements. Second, the electric impedance of the acquisition system should be tuned in order to match the internal impedance R_i of the antennas. When these conditions met, the sensed DC power reach a maximum value given by $P_{DC} = V/4R_i$ [36], where R_i is usually considered as the mean ohmic resistance of the nano-thermocouples [37]; here evaluated with the dimensions of the structures and the values 420 nΩ•m and 69.3 nΩ•m for the DC titanium and nickel resistivity, respectively.

An estimation of the efficiency η_e, exhibited by the IR detectors can then be performed by evaluating the ratio of the power that antennas generates PDC to the power by heating they absorb Q_V (obtained by integrating the heat-power density over the volume of the antennas). The internal resistance, DC power, resistive heating and conversion efficiency were evaluated for some specific cases and presented in Table 2.

Table 2. Efficiency of three types of Seebeck nanoantennas at λ = 10.6μm

Nano-structure	*Mean R_i (Ω)*	*P_{DC} (fW)*	*Q_V (μW)*	*η_e (%)*
Square spiral(RCHP)	*~490*	*~0.016*	*~0.79*	*~2×10^{-9}*
Archimedean spirals (RCHP)	*~820*	*~4.45*	*~2.98*	*~0.15×10^{-6}*
Single loop (LP 0°)	*~136*	*~260*	*~1.4*	*~18.5×10^{-6}*

The efficiencies values that Seebeck nanoantennas reach range from 10^{-9} to $10^{-5\%}$. These values are 1 to 10^3 greater than the efficiency of the reported rectifying nanoantennas counterpart [20,22]. The efficiency of the rectifying antennas is drastically decreased because two mechanisms of losses are conjugated, the impedance matching between the tunnel barrier and the antenna, and the poor diode-like performance of the tunnel barriers. By using Seeebek nanoantennas not impedance losses are seen, increasing this manner the nanoantennas overall performance. However, the efficiencies of the proposed IR detectors remain low because of the heat losses through the substrate. These losses could be reduced by using air-bridge technologies.

4. Conclusions

The response of a series of Seebeck nanoantennas to convert the optical power of radiation at λ = 10.6μm into DC power was evaluated by using thermal numerical simulations, showing that devices represent an alternative for infrared sensing (exploiting the optical energy naturally dissipated as heat). Numerical simulations show a voltage responsivity of 112 mV/W for these Seebeck nanoantennas, this value can be increased by reducing the effective thermal conductivity of the substrate. This can be achieved by suspending the device on air above its substrate. Moreover, engineering of large phase-arrays of nano-antennas acting as series thermocouples arrays can also be implemented to increase the voltage output and the capture area of the devices.

When considering Seebeck nanoantennas for the characterization of the state of polarization, the use of the Seebeck effect is well suited to provide a signal that can be related with the difference in power of two orthogonal components of the electric field. This has been demonstrated numerically for an arrangement of two Archimedean Seebeck nanoantennas. This element is sensitive to levo and dextro polarization states and produces a signal proportional to the fourth Stokes parameter. Also the square closed-loop antenna is sensitive to linear polarization when placing the thermocouple junctions at the appropriate place.

#212448 - $15.00 USD Received 20 May 2014; revised 11 Jul 2014; accepted 14 Aug 2014; published 17 Sep 2014

Acknowledgments

This work was supported by the project “Centro Mexicano de Innovación en Energía Solar” from Fondo Sectorial CONACYT-Secretaría de Energía-Sustentabilidad Energética”, by CONACYT through postdoctoral grant CV-45809, by FONDECYT under project 3120059, by La Region Lorraine; and by Project ENE2009-013430 from the Spanish Ministerio de Innovación.

#212448 - $15.00 USD Received 20 May 2014; revised 11 Jul 2014; accepted 14 Aug 2014; published 17 Sep 2014